Network Modeling Analysis in Health Informatics and Bioinformatics (2025) 14:22
https://doi.org/10.1007/s13721-025-00515-3

ORIGINAL ARTICLE

Investigation of total-body applicable compartment models for kinetic modeling in total body ^{15}O-water perfusion PET imaging

Oona Rainio[1] · Juhani Knuuti[1] · Riku Klén[1]

Received: 12 December 2024 / Revised: 11 February 2025 / Accepted: 16 March 2025

Abstract

Dynamic total-body positron emission tomography (PET) imaging has recently become possible due to the introduction of new-generation imaging systems with increased axial field of view. This enables evaluation of kinetic modeling approaches using compartment models for the entire body simultaneously. Systematic evaluation of the conventionally used approaches is needed to find the best candidates among different compartment models for total body modeling of ^{15}O-water perfusion PET images. Six variations of the 1-tissue-compartment model (1TCM) are evaluated. The models are systematically fitted to mean time activity curves of 20 anatomic structures of interest extracted from a dynamic ^{15}O-water PET rest perfusion images of 58 human subjects, using an image-derived input function from the aorta. The impact of additional parameters for time delay correction (TDC), arterial volume fraction (AVF), and perfusable tissue fraction (PTF) is assessed. The models are evaluated with mean squared error, mean relative error (MRE), and Akaike information criterion (AIC) and by performing Wilcoxon signed-rank tests to see whether the found differences are statistically significant. For 11 out of the 20 anatomic structures, the best model in terms of median AIC was the 1TCM with AVF and TDC but without PTF. The use of TDC resulted in significantly lower AICs for all anatomic structures while the AVF and PTF parameters significantly improved the model performance only occasionally. Between the different organs, the models of pancreas, spleen, myocardium, the example rib, and brain performed very well in terms of MRE. In comparison, the investigated models worked poorly for liver and lung lobes. This paper serves as an initial attempt to evaluate potential approaches to derive an appropriate model for kinetic modeling in total body ^{15}O-water PET perfusion imaging. According to our research, the suitability of 1TCM using a single input function from the aorta in ^{15}O-water PET images depends on the organ of interest. Our results suggest that the use of 1TCM is justified for most anatomic structures and can be used to estimate the cerebral, myocardial, renal, and splenic blood flow. However, we recommend different models for quantification of hepatic and pulmonary blood flow.

Keywords Compartment modeling · Kinetic models · Total body imaging · Medical imaging · Positron emission tomography · Perfusion

1 Introduction

Positron emission tomography (PET) allows accurate imaging of body functions on a molecular level, by enabling to track and quantify the biochemical and the physical processes of different short-lived radioactive tracer substances in the human body (Townsend 2004). The results of a PET scan can be presented either as one static three-dimensional (3D) image or as a dynamic series of 3D images (4D). The strength of dynamic PET is the ability to follow the changes in the molecular processes with respect to time and quantify different kinetic measurements such as blood flow via kinetic modeling.

For a long time, kinetic modeling research in PET imaging was limited to single organs as conventional scanners were restricted to a short axial field of view (SA-FOV), up to 20 or 30 cm only (Wang et al. 2022). Recently introduced total-body PET system, or long axial FOV (LA-FOV), has enabled the simultaneous dynamic PET imaging of all the

✉ Oona Rainio
ormrai@utu.fi

Juhani Knuuti
juhani.knuuti@varha.fi

Riku Klén
riku.klen@utu.fi

[1] Turku PET Centre, University of Turku and Turku University Hospital, Turku, Finland

Published online: 09 April 2025

possible organs of interest (Knuuti et al. 2023; Wang et al. 2021), with numerous possibilities to extend the kinetic modeling schemes to entire body and multiple organs at once.

Typically, either compartmental modeling, clustering algorithms, or graphical methods are used to describe the tracer kinetics to gather quantitative information from the time-activity curve (TAC) of each voxel of the PET image or the mean TAC of a specific region of interest (ROI) or volume of interest (VOI) (Bertoldo et al. 2014). The most common of these methods, compartmental modeling, is based on the assumption that the interactions of the tracer concentration between blood and different tissues can be divided to specific compartments. Thereafter, the biochemical and physical interactions between the compartments can be described through rate constants ($K_1, k_2, \ldots$) expressing the fraction of the total tracer that will leave the compartment per unit time (Kralj 2002).

For ^{15}O-water PET, the rate constants are meaningful because they can be used to quantify blood flow in a noninvasive way (Knuuti et al. 2023). These blood flow estimates are meaningful for clinical purposes because decreased blood flow in a specific organ can be an indicate of several significant diseases and health conditions (Igarashi et al. 2021; Katayama et al. 2021; Klinge et al. 1998; Komar et al. 2009), depending on the organ in question. Because water has high first-pass extraction fraction and is metabolically and chemically inert, the most common model for ^{15}O-water is the 1-tissue compartment model (1TCM) (Rainio and Klén 2025). Additional corrections can be included for the tracer concentration in the arteries within the tissue, the non-perfusable tissue, and the time delay caused while the tracer travels from the blood input to the tissue of interest (Boellaard et al. 2005).

However, there is currently no research comparing the suitability of 1TCM between different organs in ^{15}O-water PET images. Due to the limited field of view of the SA-FOV systems, previous approaches have focused solely on single-organ modeling. Instead, the current studies related to total-body imaging are limited to assessing the tracer kinetics in ^{18}F-fluorodeoxyglucose for measurement of tissue metabolism (Wang et al. 2022), or more recently ^{11}C-Butanol for measurement of perfusion (Li et al. 2023). Unlike for ^{15}O-water, the 1TCM is not used for these tracers because their kinetics are more complex and require additional corrections for tracer metabolites.

In this article, our aim is to evaluate the applicability of the 1TCM approaches for total body dynamic ^{15}O-water PET perfusion imaging. Our goal is to find suitable candidates among the different versions of this model to provide the best fit among several organs. This information is namely needed to develop methods for simultaneous kinetic modeling of multiple organs in total-body perfusion PET studies.

2 Materials and methods

2.1 Software requirements

An automatic segmentation tool called TotalSegmentator (version: 1.0) (Wasserthal et al. 2023) was used to define the VOIs for the anatomic structures of interest from computed tomography (CT) images. The PET and CT images and the output of TotalSegmentator were visually checked with Carimas (version: 2.10) (Rainio et al. 2023). The images were pre-processed and the TACs were extracted in Python (version: 3.9.9) (van and Drake 2009), while R (version: 3.4.1) (R Core Team. 2021) was used for model parameter selection, performance evaluation of the models, and statistical testing.

2.2 Data

The data of this study was retrospectively collected from 58 patients who underwent total-body PET perfusion imaging with Biograph Vision Quadra (Siemens Healthineers) PET/CT scanner at Turku PET Centre in Turku, Finland, between August 2022 and January 2023. The inclusion criterion was a suspected coronary artery disease (CAD) due to stable chest pain and similar symptoms. The mean age of patients was 63.9 with standard deviation of 8.36 years (range: 43–81 years), their mean weight was 88.4 kg with standard deviation of 18.5 kg (range: 59.0–132 kg), and the male–female sex ratio was 29:29.

Before the imaging, the patients were injected with a dose (mean activity of 354 MBq with standard deviation of 24.2 MBq, range of [307,408] MBq) of ^{15}O-labeled water, [^{15}O]H_2O, also known as radiowater. The imaging resulted in dynamic rest PET image sequence of 24 3D images of $220 \times 220 \times 380$ voxels of $1.65 \times 1.65 \times 2.80$ mm^3 taken between time intervals 14·5 s, 3·10 s, 3·20 s, and 4·30 s, and singular CT images of $512 \times 512 \times 380$ voxels. Stress perfusion PET images were also taken for some patients, but they were not used in this study. The PET data was corrected for decay and the original voxel unit was Bq/mL. Figure 1 shows the same coronal slice from the PET image of one patient at three different time points.

The segmentation masks created with TotalSegmentator from the CT images were used to compute the mean TACs of the aorta and 20 other different anatomic structures in PET images. These 20 structures included brain, myocardium, five lung lobes (left lower lobe (LLL), right lower lobe (RLL), right middle lobe (RML), left upper lobe (LUL), and right upper lobe (RUL)), liver, spleen, pancreas, left and right kidney, colon, urinary bladder, three examples of muscle tissue (right gluteus maximus,

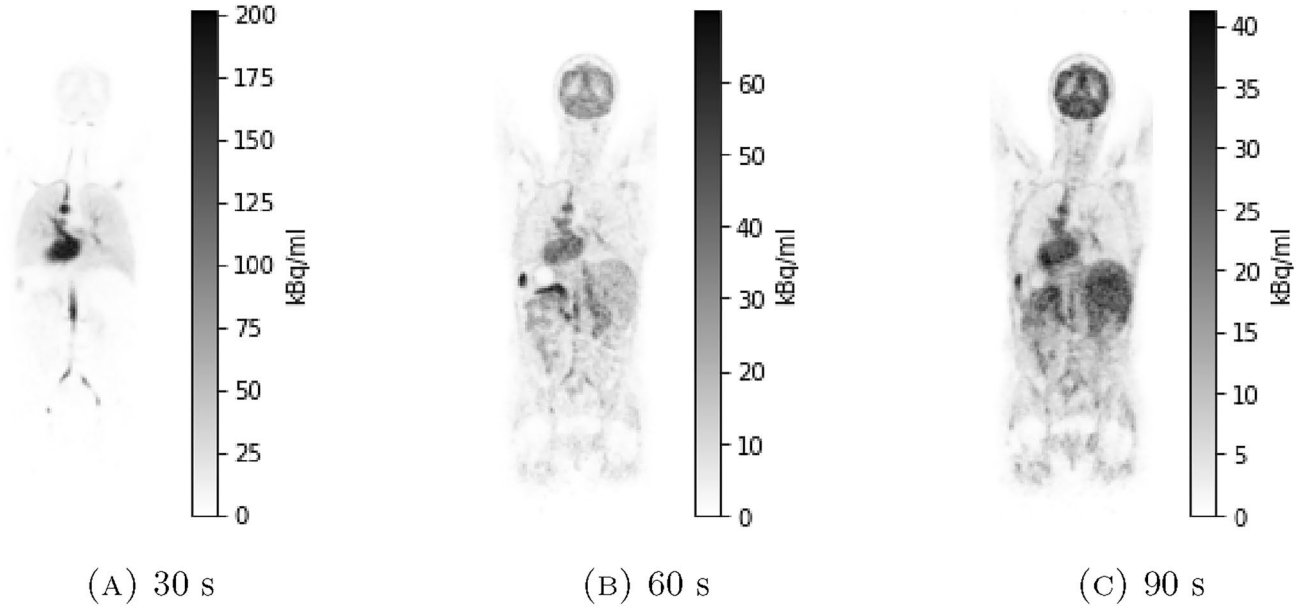

(A) 30 s (B) 60 s (C) 90 s

Fig. 1 The same coronal slice in a dynamic PET image from one patient after the specified number of seconds (s) has passed since the start of the imaging

left gluteus medius, and right iliopsoas), and three examples of bone tissue (right humerus, the 10th right rib, and T5 vertebra). To avoid potential errors from the possible incorrect segmentation of a few voxels outside the actual target, only the greatest connected component was used to compute the mean TAC. Linear interpolation was used to compute the TAC values at 1, 2,..., 280 s from the original 24 time points by assuming that the TAC value at 0 s is 0.

2.3 Compartment models

1TCM has two compartments, one for ^{15}O-water concentration in the tissue of interest and one for the ^{15}O-water concentration in the arterial blood. The activity of these compartments with respect to time t is described with two functions $C_T(t)$ and $C_A(t)$, the latter of which is the input function of the model. The ^{15}O-water is assumed to be exchanged from the arterial blood into the tissue and vice versa according to the differential equation

$$\frac{\partial}{\partial t}C_T(t) = K_1 C_A(t) - k_2 C_T(t), \tag{2.1}$$

where the rate constants K_1 and k_2 are constant with respect to time.

The arterial input function $C_A(t)$ is always directly obtained from the mean TAC of the aorta. Additionally, we can set $C_T(0) = 0$ as there is no ^{15}O-water in the body before the injection and, whenever the value of the function $C_T(t)$ is known at the time point t, we can estimate its value at the next time point $t + \Delta t$ by using the differential equation (2.1). If the rate constants are suitably chosen for the anatomic structure of interest, then the ^{15}O-water concentration in the tissue of this anatomic structure $C_T(t)$ should resemble the mean TAC of this anatomic structure.

However, the default version of the 1TCM might sometimes overestimate the perfusion if the activity in the arteries within the tissue is included in the activity measured from the tissue. To avoid this issue, we can define (Kuttner et al. 2021)

$$C_{PET}(t) = (1 - V_A)C_T(t) + V_A \cdot C_A(t), \tag{2.2}$$

where $V_A \in (0, 1)$ is the arterial volume fraction (AVF) in the tissue, and estimate the similarity of $C_{PET}(t)$ and the mean TAC instead of comparing the function $C_T(t)$ directly to the mean TAC. To account also for vasculature and non-perfusable tissue, we can alternatively consider (Lubberink et al. 2015)

$$C_{PET}(t) = \alpha(1 - V_A)C_T(t) + V_A \cdot C_A(t), \tag{2.3}$$

where $\alpha \in (0, 1)$ is the perfusable tissue fraction (PTF).

Another factor that might affect the model fit is the time delay caused by the travel of the ^{15}O-water from the site where the input is measured to the anatomic structure of interest. The time delay correction (TDC) is included by simply replacing $C_A(t)$ in the differential equation (2.1) with a value $C_A(t - j)$ dependent on an additional integer parameter j (Wang et al. 2022). If j is positive, the injected ^{15}O-water reaches the aorta before the anatomic structure of interest and the opposite is true for a negative value of j.

We study here the six model options summarized in Table 1. The number of parameters varies from 2 to 5. The rate constant K_1 is a non-negative real number expressing the amount of tracer delivery from 1 mL of arterial blood to 1 mL of tissue per second, though it will be converted into the unit mL/min/mL. The other rate constant k_2 expresses the wash-out from the tissue and has the initial unit /s converted into /min. The TDC parameter j is an integer (unit: s), and $V_A, \alpha \in (0, 1)$ describe AVF and PTF without units.

2.4 Parameter selection

The model parameters are chosen by finding optimal choices of the model parameters in terms of error. The most complicated model, 1TCM with TDC, AVF, and PTF, is fitted as follows: We initialize $C_T(0) = 0$ and consider the $n = 280$ time points of i seconds for $i = 1, 2, \dots, n$. For every $j = -30, -29, \dots, 30$, we extrapolate $C_A(-i) = 0$ for $i = 1, \dots, j$ if $j \geq 1$ and $C_A(n + i) = C_A(n)$ for $i = 1, \dots, |j| - 1$ if $j \leq -2$. By (2.1), the function $C_T(t)$ can be computed iteratively as

$$C_T(i) = K_1 C_A(i - j - 1) + (1 - k_2) C_T(i - 1), \quad i = 1, 2, \dots, n, \tag{2.4}$$

for any choices of K_1 and k_2. We define $C_{PET}(t)$ as in (2.3) for $V_A, \alpha \in (0, 1)$. The model error is measured as the sum of the squared differences

$$\sum_{i=1}^{n} (\tilde{C}(i) - C_{PET}(i))^2, \tag{2.5}$$

where $\tilde{C}(t)$ is the measured mean TAC of the anatomic structure of interest. We use the non-linear Newton-type minimization algorithm called `nlm` in R to find the optimal choices for the model parameters by minimizing this error term for every $j = -30, -29, \dots, 30$. Since `nlm` does not allow constraints for the optimization, we optimize parameters $u_1, u_2, u_3, u_4 \in (-\infty, \infty)$ such that

$$K_1 = |u_1|, \quad k_2 = |u_2|, \quad V_A = \frac{1}{1 + e^{-u_3}}, \quad \alpha = \frac{1}{1 + e^{-u_4}}$$

to ensure that $K_1, k_2 \in [0, \infty)$ and $\alpha, V_A \in (0, 1)$. We initialize $u_1 = u_2 = 0.01$, $u_3 = -\log(9)$, and $u_4 = \log(9)$. After the optimization, we choose the value of j with lowest error term (2.5). All the other models work similarly except for one or more of their parameters are not optimized but instead fixed as zeros or, in case of α, as 1 to remove them from the model.

Table 1 Model parameters for six different model options including 1TCM with no additional parameters, with arterial volume fraction (AVF) only, with AVF and perfusable tissue fraction (PTF), with time delay correction (TDC) only, with TDC and AVF, and with TDC, AVF, and PTF

	No AVF nor PTF	AVF only	AVF+PTF
No TDC	K_1, k_2	K_1, k_2, V_A	K_1, k_2, V_A, α
TDC	K_1, k_2, j	K_1, k_2, V_A, j	K_1, k_2, V_A, α, j

2.5 Evaluation of the models

To estimate the model error, we compute mean squared error (MSE) and mean relative error (MRE) defined as

$$\text{MSE} = \frac{1}{n} \sum_{i=1}^{n} (\tilde{C}(i) - C_{PET}(i))^2 \quad \text{and}$$

$$\text{MRE} = \frac{1}{n} \sum_{i=1}^{n} \frac{|\tilde{C}(i) - C_{PET}(i)|}{\tilde{C}(i)}, \quad n = 280.$$

The reason for using all the 280 interpolated time points here instead of just the original 24 ones is that we want to give equal weight of the whole interval. Given the models with most parameters are expected to fit the data better than the others, we use Akaike information criterion (AIC) defined as (Burnham and Anderson 2004)

$$\text{AIC} = n \log(\text{MSE}) + 2N$$

to determine whether the difference in the model performance is great enough to justify the increased complexity of the model. Here, the number of estimated parameters N can be calculated from Table 1. The model with the lowest AIC is considered to be the best. We use Wilcoxon signed-rank test with the standard level of significance of 5% to estimate whether a model produces significantly lower AICs than a different model from the same anatomic structure or significantly lower MREs than a model from a different anatomic structure. We test here MREs instead of the MSEs because, unlike MSEs, the MREs are not affected the differences in the tracer uptake between the anatomic structures.

3 Results

3.1 Best model for each organ

Table 2 shows the best model for each anatomic structure in terms of median AIC and the p-values of the Wilcoxon signed-rank tests used to estimate if the best model produces significantly lower AICs than the other models for the same anatomic structure. The best model always included TDC and most often also AVF but not PTF. Based on the p-values of Table 2, we see that the use of TDC significantly decreased the AICs of the best-performing models and PTF increased them, whereas the choice to include the

Table 2 The best model in terms of median AIC for each anatomic structure and the p-values denoted by using * if p-value≤0.05, ** if p-value≤ 0.01, or *** if p-value≤0.001 for the Wilcoxon signed-rank tests comparing whether the specified best model produces significantly lower AICs than the 1TCM with different choices regarding to AVF (denoted here with the parameter V_A), PTF (the parameter α), and TDC

Anatomic structure	Best model	>1TCM	>1TCM+ V_A	>1TCM+ V_A+α	>1TCM+ TDC	>1TCM+ V_A+TDC	>1TCM+ V_A+α+TDC
Aorta	1TCM+V_A+α+TDC	***	***	***			–
Brain	1TCM+V_A+TDC	***	***	***	***	–	***
Myocardium	1TCM+V_A+TDC	***	***	***		–	***
LLL	1TCM+V_A+TDC	***	***	***	*	–	***
RLL	1TCM+TDC	***	***	***	–	**	***
RML	1TCM+V_A+TDC	***	***	***		–	***
LUL	1TCM+V_A+TDC	***	***	***		–	***
RUL	1TCM+V_A+α+TDC	***	***	***	***		–
Liver	1TCM+V_A+TDC	***	***	***	***	–	**
Spleen	1TCM+TDC	***	***	***	–		
Pancreas	1TCM+TDC	***	***	***	–	*	***
Kidney, L	1TCM+TDC	***	***	***	–	***	***
Kidney, R	1TCM+V_A+TDC	***	***	***		–	***
Colon	1TCM+V_A+TDC	***	***	***	***	–	***
Bladder	1TCM+TDC	***	***	***	–	**	***
Glu.max., R	1TCM+TDC	***	***	***	–		***
Glu.med., L	1TCM+V_A+TDC	***	*	***	***	–	***
Iliopsoas, R	1TCM+V_A+TDC	***	***	***	***	–	***
Humerus, R	1TCM+V_A+α+TDC	***	***	***	***		–
10th rib, R	1TCM+V_A+TDC	***	***	***	***	–	***

No symbol means that a Wilcoxon test was run but the p-value was over 0.05 and the symbol – means that no test was run because the best model is the one in the column

AVF in the model rarely produced significant differences in the AICs.

3.2 Fitted parameters and error estimates

The median values of the parameters of the best models are reported in Table 3. We see that the fitted rate constants K_1 and k_2 were very high for some lung lobes. The PTF parameter α had always a median of 0.90 equal to the initial value, suggesting that it did not converge from this for most of the patients, not even for the organs where including the PTF decreased the AICs on average. Additionally, while it is credible that the tracer reaches myocardium and lung lobes before the aorta, the 10th rib also had a negative value of the time parameter j. The related error terms are in Table 4, which show that the models did not fit very well to lung lobes, liver, and kidneys.

3.3 Model fit compared between the organs

Finally, Table 5 summarizes the p-value of the Wilcoxon signed-rank tests comparing whether the best model of a specific anatomic structure produces significantly lower MREs than the best model of another anatomic structure. Pancreas, spleen, 10th rib, and myocardium had significantly lower MREs than any other anatomic structure. In addition to these organs, the models of brain, three example muscles, and two other example bones besides the 10 the rib also produced significantly less MRE than most of the other models. In comparison, the models of lower and middle lung lobes and liver performed poorly. Examples of fitted models can be seen from Fig. 2.

4 Discussion

To our knowledge, this study was the first to investigate the total body applicability of 1TCM for kinetic modeling of ^{15}O-water perfusion PET studies. Our topic of study has not been possible before because the introduction of LA-FOV PET systems only recently enabled the simultaneous imaging data of tissue perfusion around the whole human body. Our study serves as a baseline to see which of the possible variations of 1TCM produce the best fit for the individual tissues as well as the values of the fitted model parameters for 20 different organs. We hope that our results benefit both for those researching universal voxe-wise models for total-body PET images and those focusing on the modeling of a single organ of interest.

By comparing Tables 2 and 6, it can be seen that the values of the fitted rate constant K_1 for brain, myocardium, spleen, and kidneys in our research resemble the reported

Table 3 The median values of the fitted model parameters of the best model (see Table 2) and the ratio K_1/k_2 over all the 58 patients for each anatomic structure separately

Anatomic structure	K_1 (mL/min/mL)	k_2 (/min)	K_1/k_2	V_A (%)	α (%)	j (s)
Brain	0.590	0.563	1.03	0.294	90.0	0
Myocardium	1.02	1.02	0.994	10.0		−12.5
LLL	1.95	5.47	0.347	0.619		−11
RLL	2.10	5.73	0.343	0.0203		−13
RML	5.79	20.4	0.263			−9
LUL	8.88	33.4	0.291	0.000632		−8
RUL	13.1	41.4	0.309	6.27e−05		−8
Liver	0.65	0.584	1.13	4.99	90.0	21
Spleen	1.58	1.65	0.998	3.7		3
Pancreas	1.38	1.54	0.869			1
Kidney, L	2.17	2.50	0.851			0.5
Kidney, R	2.18	2.54	0.837			1
Colon	0.134	0.428	0.307	0.0676		1
Bladder	0.027	0.268	0.107	0.135		1
Glu.max., R	0.0648	0.158	0.457			3
Glu.med., L	0.0874	0.19	0.573			4
Iliopsoas, R	0.0808	0.186	0.425	0.692		0
Humerus, R	0.0449	0.236	0.185	0.308		0
10th rib, R	0.140	0.339	0.431	2.41	90.0	−13
T5 vertebra	0.125	0.290	0.457	2.6		5

If no value is given, the parameter was not present in the best model

Table 4 Median values of MSE (computed between curves with unit Bq/mL), MRE, and AIC for the best model (see Table 2) for the given anatomic structure

Anatomic stricture	MSE	MRE	AIC
Brain	46,700	0.0720	3020.64
Myocardium	396,000	0.0563	3616.69
LLL	360,000	0.253	3590.54
RLL	645,000	0.320	3753.55
RML	195,000	0.162	3416.3
LUL	107,000	0.114	3251.79
RUL	132,000	0.0812	3308.39
Liver	772,000	0.131	3805.97
Spleen	279,000	0.0701	3519.02
Pancreas	151,000	0.0700	3344.34
Kidney, L	793,000	0.132	3809.49
Kidney, R	907,000	0.134	3847.06
Colon	18,400	0.0914	2756.79
Bladder	2350	0.100	2181.44
Glu.max., R	2310	0.0844	2174.94
Glu.med., L	4590	0.0892	2365.01
Iliopsoas, R	11,600	0.0890	2629.17
Humerus, R	2490	0.0874	2197.23
10th rib, R	22,600	0.0668	2816.95
T5 vertebra	26,300	0.0796	2857.7

estimates of cerebral, myocardial, splenic, and renal blood flow from earlier ^{15}O-water PET research (Aanerud et al. 2017; Heijtel et al. 2014; Inaba et al. 1989; Kudomi et al. 2009; Lubberink et al. 2010; Nesterov et al. 2009; Taniguchi et al. 1999; Zhang et al. 2014), respectively. Additionally, the values of the ratio K_1/k_2 are also very close to 1 for brain and spleen, which suits the common estimate of the water partition coefficient. The values of K_1 for three example muscles are higher than the blood flow values in the femoral (Malminiemi et al. 1997) and the lower leg muscles (Christensen et al. 2024) reported earlier, but we also use gluteus muscles and iliopsoas as our examples instead of the leg muscles.

On the contrary, our research suggest that the investigated versions of the 1TCM are not ideal for lung lobes and liver. This is expected because the arterial input function is not realistic for neither of these organs. Namely, lungs receive the majority of their blood supply from the pulmonary circulation as opposed to the systemic circulation passing through the aorta. Consequently, Schuster et al. (1995) used the input function defined in the right ventricular cavity instead of the aorta. In addition to this, the current lung VOIs produced by TotalSegmentator include both several large pulmonary arteries and air within the lungs. While we initially wished that the impact of these factors could be accounted by the AVF and the PTF corrections, it seems that the adjustment of the VOIs

Table 5 The p-values denoted by using * if p-value≤0.05, ** if p-value≤0.01, or *** if p-value≤0.001 for the Wilcoxon signed-rank tests comparing whether the best model (see Table 2) of the anatomic structure on a given row produces significantly lower MREs for the 58 patients than the the best model of the anatomic structure in column

	Brain	Myocardium	LLL	RLL	RML	LUL	RUL	Liver	Spleen	Pancreas	Kidney, L	Kidney, R	Colon	Bladder	Glu. max., R	Glu. med., L	Iliopsoas, R	Humerus, R	10th rib, R	T5 vertebra
Brain	–		***	***	***	***	***	***			***	***	***	***	***	***	***	***		
Myocardium		–	***	***	***	**	**	***			***	***	**	**	*	**	*	**		
LLL			–	***																
RLL				–																
RML			***	***	–															
LUL			***	***	***	–														
RUL			***	***	***	*	–	**			***	***								
Liver			***	***	**			–				*								
Spleen			***	***	***	***	**	***	–		***	***	***	***	***	***	***	***		**
Pancreas	*		***	***	***	***	**	***		–	***	***	***	***	***	***	***	***		**
Kidney, L			***	***	**						–	*								
Kidney, R			***	***	*							–								
Colon			***	***	***	**		***			***	***	–	**						
Bladder			***	***	***	*		***			***	***		–						
Glu.max., R			***	***	***	***		***			***	***		**	–					
Glu.med., L			***	***	***	***		***			***	***		**		–				
Iliopsoas, R			***	***	***	**		***			***	***		**			–			
Humerus, R			***	***	***	*		***			**	**		*				–		
10th rib, R			***	***	***	***	**	***			***	***	**	***	**	**	**	**	–	*
T5 vertebra			***	***	***	***		***			***	***	***	***	*	**	*	*		–

No symbol means no significant p-value and the symbol – that the column and the row are the same

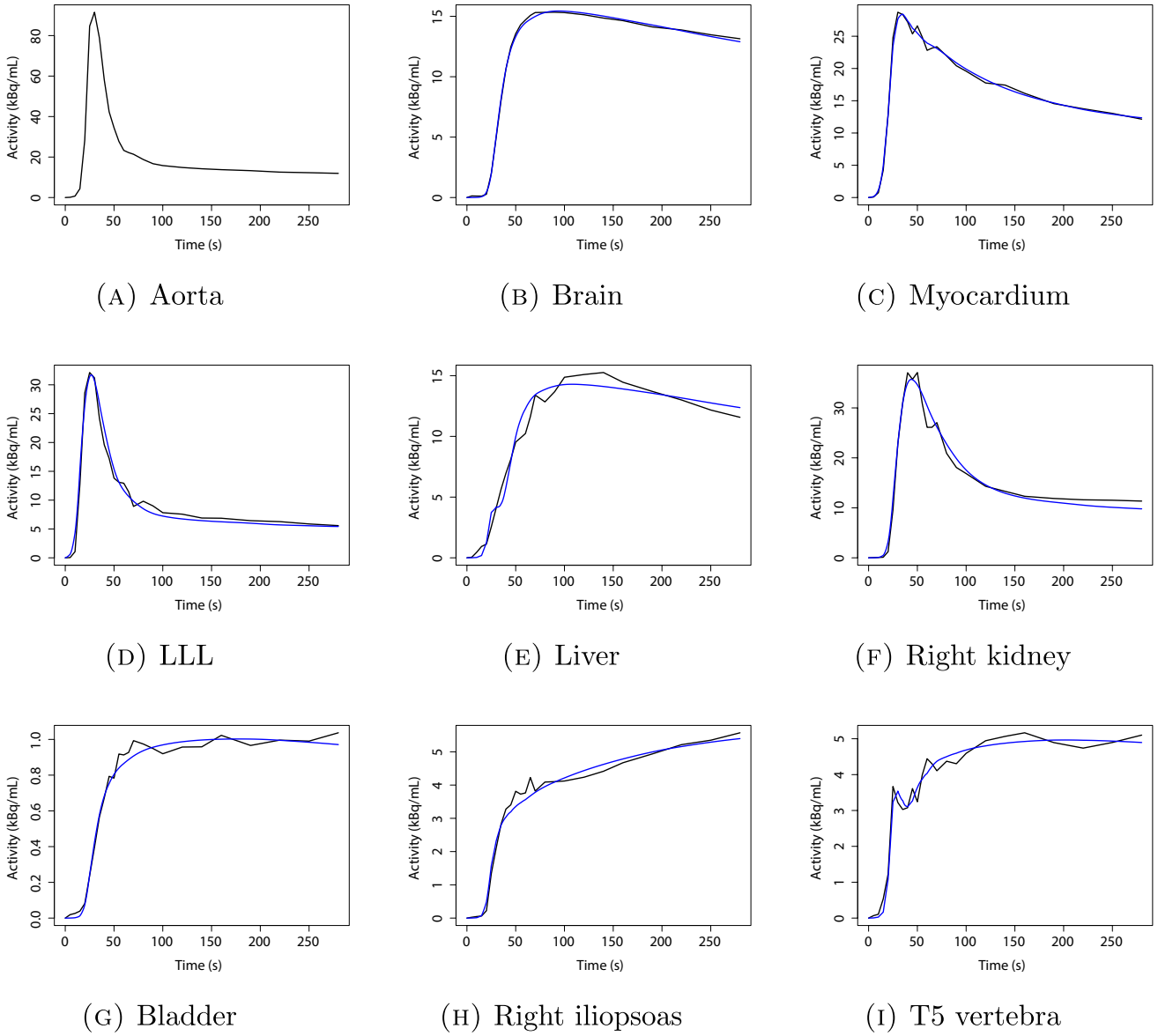

Fig. 2 The TACs of nine different anatomic structures in black line from one example patient. Except for the aorta whose TAC is used as the input function in the models, the fitted best models (see Table 2) are also plotted in blue line

would be needed instead, to avoid too high perfusion estimates for the upper lung lobes.

Liver receives the majority of its blood from the portal vein instead of the hepatic artery (Sureka et al. 2015), which is why a special dual-input model has been suggested for liver instead of the 1TCM by Taniguchi et al. (1999). Compared to the tracer delivery from the hepatic artery, the portal vein delivery is dispersed and delayed in time because the tracer travels through other organs before reaching the liver. Consequently, the use of 1TCM produces too high perfusion estimate for the arterial delivery and misplaces its peak, as can be noted from the high value of the delay parameter j in Table 3.

According to our results, 1TCM did not work especially well for kidneys, either, possibly due to their complex blood flow structure and functional differences between the kidney core and medulla. They likely would benefit from a multi-compartment model separating the cortex and the medulla or we should estimate cortical and medullary flow separately. Still, our renal blood flow estimates were still relatively reasonable in comparison with those in Table 6. Similarly, a specific model could be designed for the urinary bladder to account for both the ^{15}O-water in the bloodstream and the urine coming from the kidneys.

There was notably differences within both the three example muscles and the three example bones. For instance,

Table 6 Blood flow estimates reported in earlier research

Blood flow	Estimate	Subjects	Research
Gray-matter cerebral	0.47±0.023	Healthy women at 65 years	Aanerud et al. (2017)
Global cerebral	0.485±0.056	16 healthy volunteers	Heijtel et al. (2014)
Gray-matter cerebral	0.518±0.077	10 healthy volunteers	Zhang et al. (2014)
Myocardial	0.96±0.42	25 patients with suspected CAD	Lubberink et al. (2010)
Myocardial	0.988±0.275	48 patients with suspected CAD	Nesterov et al. (2009)
Renal	1.71±0.61	8 healthy volunteers	Inaba et al. (1989)
Renal	3.11±1.48	6 healthy volunteers	Kudomi et al. (2009)
Pulmonary	1.41±0.22	15 healthy volunteers	Schuster et al. (1995)
Hepatic	1.293	88 patients	Taniguchi et al. (1999)
Splenic	1.333	88 patients	Taniguchi et al. (1999)
Femoral muscle	0.034±0.003	5 healthy volunteers	Malminiemi et al. (1997)
Lower leg muscles	0.0213	10 healthy volunteers	Christensen et al. (2024)

The estimate is either the mean ± standard deviation or just the mean or the median, and has the unit mL/min/g for all other research except of Christensen et al. (2024) and Schuster et al. (1995) where the unit is mL/min/mL. While we also use the unit mL/min/mL, 1 mL or 1 cm^3 of tissue weights around 1 g, so converting the values between units does not change them much

adding the AVF parameter to the 1TCM with TDC significantly decreased the AICs for the left gluteus medium but not for the right gluteus maximus. Also, unlike the other bone and muscle examples, the model of the 10th rib had a negative time delay, meaning that the tracer would reach the rib before the aorta, and this model also produced significantly lower MREs than the best models of the other organs. This perhaps raises questions about how accurate the segmentation was and, in particular, whether respiratory motion produced error the segmentation of the 10th rib. Naturally, more in-depth analysis for the suitability of the compartment models for muscle or bone tissue would require more muscle and bone examples and more careful evaluation whether the segments are correctly placed.

We briefly checked the possible impact of the initial values of our parameters. We noted that the optimization algorithm produced consistently the same values of K_1 and k_2, regardless of their initial values. However, the additional parameters V_A and α were sensitive to their initial values. In particular, the value of α often stayed very close its initial value, suggestion that the PTF correction leads to over-parametrized models. Furthermore, while we fitted the models by giving an equal weight to all the 280 linearly interpolated time points, a different choice can be made if the aim is to find such a model that fits the peak or the end of the TAC better.

In our study, we performed the segmentation via the automatic CT-based segmentation tool, TotalSegmentator. It should be taken into account that the use of this tool might have caused some segmentation errors that could have affected in the final results. However, we performed compartment modeling in over 20 organs of interest for a relatively large patient population and this type of comprehensive analysis it is only feasible in combination TotalSegmentator or another alternative automatic tool. Additionally, the benefit of TotalSegmentator is that it directly produces a 3D VOI unlike the physicians who often draw a single two-dimensional ROI or combine a few ROIs to produce a rough interpolation of the 3D VOI (Rainio and Klén 2025). Since we do not consider all the voxels in the 3D VOI but rather their mean TAC, the potential bias from incorrect voxels is small. On the other hand, there is likely some misalignment between the initial CT image and different time-frames of the dynamic PET images due to the motion of the patient, which might cause spill-over between organs or underestimation of the mean TACs.

One of the possible subjects of future study is creating a larger compartment model with several anatomic structures in the same model. Since we have information about the whole body, we could study for example how the tracer travels from the heart or other organs to the kidneys and from the kidneys to the urinary bladder. Similarly, lung lobes could be perhaps better described with one model rather than five models for each lobe. The potential of the 2-tissue compartment model could also be investigated for ^{15}O-water. Namely, even though the water is metabolically inert, its behavior in the tissue could be described by dividing it between a fast-moving and a more slow-moving component. Additionally, it could be studied how the stress caused by the adenosine infusion during the PET imaging affects the model performance.

5 Conclusion

For mean TACs of 20 different anatomic structures in the ^{15}O-water PET images of 58 patients, we fitted six different variations of the 1TCM with and without certain additional

parameters defining AVF, PTF, and TDC. According to our results, 1TCM with AVF and TDC was the best model in terms of median AIC for most anatomic structures. TDC significantly improved the model performance whereas the impact of AVF was significant only for less than half of the anatomic structures considered. By comparing MREs between different anatomic structures, it was noted that the compartment model fit the best for pancreas, spleen, myocardium, and the example rib, closely followed by brain. Significantly higher MREs were obtained from liver and lung lobes. The fitted rate constants in the models of brain, myocardium, spleen, and kidneys were also harmonic with earlier estimates of cerebral, myocardial, splenic, and renal blood flow.

Acknowledgements The authors wish to thank the reviewers for their feedback and constructive suggestions.

Funding Open Access funding provided by University of Turku (including Turku University Central Hospital). The first author was financially supported by the Finnish Cultural Foundation.

Data availability The patient data is not available due to privacy restrictions.

Code availability Available at www.github.com/rklen/Compartment_modelling_for_different_organs.

Declarations

Conflict of interest J.K. received consultation fees from GE Healthcare and AstraZeneca and speaker fees from GE Healthcare, Bayer, Lundbeck, Boehringer-Ingelheim, Pfizer, Merck, and Siemens, outside the submitted work.

Informed consent and ethical approval All the patients were at least 18 years of age, consented to the use of their data, and the research from their data was approved by Ethics Committee of the Hospital District of Southwest Finland.

References

Aanerud J, Borghammer P, Rodell A, Jonsdottir KY, Gjedde A (2017) Sex differences of human cortical blood flow and energy metabolism. J Cerebr Blood Flow Metab 37(7):2433–2440

Bertoldo A, Rizzo G, Veronese M (2014) Deriving physiological information from PET images: from SUV to compartmental modelling. Clin Transl Imaging 2:239–251

Boellaard R, Knaapen P, Rijbroek A, Luurtsema GJ, Lammertsma AA (2005) Evaluation of basis function and linear least squares methods for generating parametric blood flow images using 15 O-water and positron emission tomography. Mol Imaging Biol 7:273–285

Burnham KP, Anderson DR (2004) Multimodel inference: understanding AIC and BIC in model selection. Sociol Methods Res 33(2):261–304

Christensen NL, Sørensen J, Bouchelouche K, Madsen MA, Buhl CS, Tolbod LP (2024) Repeatability of [15O] H2O PET imaging for lower extremity skeletal muscle perfusion: a test-retest study. EJNMMI Res 14(1):11

Heijtel DF, Mutsaerts HJ, Bakker E, Schober P, Stevens MF, Petersen ET, Nederveen AJ (2014) Accuracy and precision of pseudo-continuous arterial spin labeling perfusion during baseline and hypercapnia: a head-to-head comparison with 15O H2O positron emission tomography. Neuroimage 92:182–192

Igarashi C, Okazawa H, Islam MM, Tsujikawa T, Higashino T, Isozaki M, Kikuta KI (2021) Differences in hemodynamic alteration between atherosclerotic occlusive lesions and moyamoya disease: a quantitative 15O-PET study. Diagnostics 11(10):1820

Inaba T, Yamashita M, Kawase Y, Nakahashi H, Watanabe H (1989) Quantitative measurement of renal plasma flow by positron emission tomography with oxygen-15 water. Tohoku J Exp Med 159(4):283–289

Katayama D, Yanagawa M, Matsunaga K, Watabe H, Watabe T, Kato HH et al (2021) Greater reductions in blood flow after anti-angiogenic treatment in non-small cell lung cancer patients are associated with shorter progression-free survival. Sci Reports 11(1):6805

Klinge P, Fischer J, Brinker T, Heissler HE, Burchert W, Berding G, Samii M (1998) PET and CBF studies of chronic hydrocephalus: a contribution to surgical indication and prognosis. J Neuroimaging 8(4):205–209

Knuuti J, Tuisku J, Kärpijoki H, Iida H, Maaniitty T, Latva-Rasku A, Oikonen V, Nesterov S, Teuho J, Jaakkola MK, Klén R, Louhi H, Saunavaara V, Nuutila P, Saraste A, Rinne J, Nummenmaa L (2023) Quantitative Perfusion Imaging with Total-Body PET. J Nucl Med 64(Supplement 2):11S-19S

Komar G, Kauhanen S, Liukko K, Seppänen M, Kajander S, Ovaska J, Minn H (2009) Decreased blood flow with increased metabolic activity: a novel sign of pancreatic tumor aggressiveness. Clin Cancer Res 15(17):5511–5517

Kralj L (2002) Kinetic modeling in positron emission tomography (PET). QJ Nucl Med 46:70–85

Kudomi N, Koivuviita N, Liukko KE, Oikonen VJ, Tolvanen T, Iida H, Nuutila P (2009) Parametric renal blood flow imaging using [15 O] H 2 O and PET. Eur J Nucl Med Mol Imaging 36:683–691

Kuttner S, Wickstrøm KK, Lubberink M, Tolf A, Burman J, Sundset R, Axelsson J (2021) Cerebral blood flow measurements with 15O-water PET using a non-invasive machine-learning-derived arterial input function. J Cerebral Blood Flow Metab 41(9):2229–2241

Li EJ, López JE, Spencer BA, Abdelhafez Y, Badawi RD, Wang G, Cherry SR (2023) Total-body perfusion imaging with [11C]-butanol. J Nucl Med 64(11):1831–1838

Lubberink M, Harms HJ, Halbmeijer R, de Haan S, Knaapen P, Lammertsma AA (2010) Low-dose quantitative myocardial blood flow imaging using 15O-water and PET without attenuation correction. J Nucl Med 51(4):575–580

Lubberink M, Golla SS, Jonasson M, Rubin K, Glimelius B, Sörensen J, Nygren P (2015) 15O-Water PET Study of the effect of imatinib, a selective platelet-derived growth factor receptor inhibitor, Versus

Anakinra, an IL-1R antagonist, on water-perfusable tissue fraction in colorectal cancer metastases. J Nucl Med 56(8):1144–1149

Malminiemi K, Laine H, Knuuti MJ, Ruotsalainen U, Oikonen V, Haaparanta M, Nuutila P (1997) Acute effects of celiprolol on muscle blood flow and insulin sensitivity: studies using [15O]-water,[18F]-fluorodeoxyglucose and positron emission tomography. Eur J Clin Pharmacol 52:19–26

Nesterov SV, Han C, Mäki M, Kajander S, Naum AG, Helenius H, Knuuti J (2009) Myocardial perfusion quantitation with 15 O-labelled water PET: high reproducibility of the new cardiac analysis software (Carimas ™). Eur J Nucl Med Mol Imaging 36:1594–1602

R Core Team (2021) R: A language and environment for statistical computing. R Foundation of Statistical Computing, Vienna

Rainio O, Klén R (2025) Compartmental modeling for blood flow quantification from dynamic 15 O-water PET images of humans: a systematic review. Ann Nucl Med 39(3):231–246

Rainio O, Han C, Teuho J, Nesterov SV, Oikonen V, Piirola S, Laitinen T, Tättäläinen M, Knuuti J, Klén R (2023) Carimas: an extensive medical imaging data processing tool for research. J Digit Imaging 36(4):1885–1893

Schuster DP, Kaplan JD, Gauvain K, Welch MJ, Markham J (1995) Measurement of regional pulmonary blood flow with PET. J Nucl Med 36(3):371–377

Sureka B, Patidar Y, Bansal K, Rajesh S, Agrawal N, Arora A (2015) Portal vein variations in 1000 patients: surgical and radiological importance. Br J Radiol 88(1055):20150326

Taniguchi H, Yamaguchi A, Kunishima S, Koh T, Masuyama M, Koyama H, Yamagishi H (1999) Using the spleen for time-delay correction of the input function in measuring hepatic blood flow with oxygen-15 water by dynamic PET. Ann Nucl Med 13:215–221

Townsend DW (2004) Physical principles and technology of clinical PET imaging. Ann Acad Med Singap 33(2):133–45

van Rossum G, Drake FL (2009) Python 3 Reference Manual. CreateSpace

Wang Y, Li E, Cherry SR, Wang GG (2021) Total-body PET kinetic modeling and potential opportunities using deep learning. PET Clin 16(4):613–625

Wang G, Nardo L, Parikh M, Abdelhafez YG, Li E, Spencer BA, Qi J, Jones T, Cherry SR, Badawi RD (2022) Total-body PET multiparametric imaging of cancer using a voxelwise strategy of compartmental modeling. J Nucl Med 63(8):1274–1281

Wasserthal J, Breit H-C, Meyer MT, Pradella M, Hinck D, Sauter AW, Heye T, Boll DT, Cyriac J, Yang S, Bach M, Segeroth M (2023) TotalSegmentator: robust segmentation of 104 anatomic structures in CT images. Radiol Artif Intell 5(5):e230024

Zhang K, Herzog H, Mauler J, Filss C, Okell TW, Kops ER, Shah NJ (2014) Comparison of cerebral blood flow acquired by simultaneous [15O] water positron emission tomography and arterial spin labeling magnetic resonance imaging. J Cerebr Blood Flow Metab 34(8):1373–1380